Iron Oxide as an MRI Contrast Agent for Cell Tracking

Supplementary Issue: New Concepts in Magnetic Resonance as Applied to Cellular and In Vivo Applications

Daniel J. Korchinski[1,2], May Taha[1], Runze Yang[1,2], Nabeela Nathoo[1,2] and Jeff F. Dunn[1–3]

[1]Department of Radiology, Cumming School of Medicine, University of Calgary, Calgary, Alberta, Canada. [2]Hotchkiss Brain Institute, Cumming School of Medicine, University of Calgary, Calgary, Alberta, Canada. [3]Experimental Imaging Centre, Cumming School of Medicine, University of Calgary, Calgary, Alberta, Canada.

ABSTRACT: Iron oxide contrast agents have been combined with magnetic resonance imaging for cell tracking. In this review, we discuss coating properties and provide an overview of ex vivo and in vivo labeling of different cell types, including stem cells, red blood cells, and monocytes/macrophages. Furthermore, we provide examples of applications of cell tracking with iron contrast agents in stroke, multiple sclerosis, cancer, arteriovenous malformations, and aortic and cerebral aneurysms. Attempts at quantifying iron oxide concentrations and other vascular properties are examined. We advise on designing studies using iron contrast agents including methods for validation.

KEYWORDS: magnetic resonance imaging, iron oxide, contrast agent, cell tracking

SUPPLEMENT: New Concepts in Magnetic Resonance as Applied to Cellular and In Vivo Applications

CITATION: Korchinski et al. Iron Oxide as an MRI Contrast Agent for Cell Tracking. *Magnetic Resonance Insights* 2015:8(S1) 15–29 doi:10.4137/MRI.S23557.

TYPE: Review

RECEIVED: June 3, 2015. **RESUBMITTED:** August 17, 2015. **ACCEPTED FOR PUBLICATION:** August 19, 2015.

ACADEMIC EDITOR: Sendhil Velan, Editor in Chief

PEER REVIEW: Three peer reviewers contributed to the peer review report. Reviewers' reports totaled 1441 words, excluding any confidential comments to the academic editor.

FUNDING: This paper was produced with support from an Alberta Innovates Health Solutions CRIO team grant and a Discovery grant from the National Sciences and Engineering Research Council of Canada. The authors confirm that the funder had no influence over the study design, content of the article or selection of this journal.

COMPETING INTERESTS: Authors disclose no potential conflicts of interest.

CORRESPONDENCE: dunnj@ucalgary.ca

Paper subject to independent expert blind peer review. All editorial decisions made by independent academic editor. Upon submission manuscript was subject to anti-plagiarism scanning. Prior to publication all authors have given signed confirmation of agreement to article publication and compliance with all applicable ethical and legal requirements, including the accuracy of author and contributor information, disclosure of competing interests and funding sources, compliance with ethical requirements relating to human and animal study participants, and compliance with any copyright requirements of third parties. This journal is a member of the Committee on Publication Ethics (COPE).

Published by Libertas Academica. Learn more about this journal.

Introduction

Magnetic resonance imaging (MRI) has been combined with various contrast agents to enhance tissue contrast. Iron oxide nanoparticles are largely used as a negative contrast agent, causing hypointense contrast.[1,2] Per mole, iron-based contrast is generally stronger than gadolinium (Gd), the most common contrast agent.[3]

MRI cell tracking was introduced in 1993 to look at cell survival and migration after grafting.[4] In 2001, the first in vivo time course of cell migration was reported.[5] As the field developed, in vivo studies tracking cells—eg, neural cells,[4] stem cells,[5] and dendritic cells (DCs)[6]—became increasingly popular. The strength of iron oxide is such that researchers have even succeeded in tracking single cells in vivo.[7–9]

The flexibility of iron oxide particles cannot be understated; they have been used to target specific molecules,[10] track and deliver therapeutic drugs,[11,12] label cancer vaccine effecting cells,[6] track inflammation,[13] visualize organs[14] and vasculature,[15] and heat and kill cancers.[16]

Iron oxide particles come in a range of types and sizes, including ultrasmall superparamagnetic particles of iron oxide (USPIOs; 5–50 nm), superparamagnetic iron oxide particles (SPIOs; 50–150 nm),[1] and micron-sized iron oxide particles (MPIOs), such as Bangs MC03F particles (≈1 μm).

Coating Properties

Iron nanoparticles interact with each other magnetically and via van der Waals' interactions. These interactions cause iron nanoparticles to flocculate. This flocculation may be overcome by coating the iron nanoparticles.[17] As clumping is undesirable for imaging applications and makes cell labeling difficult, in biological applications, iron nanoparticles are typically coated.[5] Flocculation can often be predicted by the nanoparticles zeta potential, the potential at its shear layer.[18] Nanoparticles that have strong negative or positive zeta potentials tend to repel and, hence, do not flocculate.[18] The zeta potential is dependent on environmental conditions (eg, pH, temperature, and solvent composition); hence, flocculation is somewhat environment-dependent. The internalization of iron nanoparticles within cells may change both the cells' and the nanoparticles' zeta potentials.[19] Negatively charged coatings may have a positive zeta potential, and vice versa. Negatively charged coatings have been reported as having superior ex vivo uptake.[20–23] Positively charged coatings have also been used to a great extent.[24–28] In an in vivo setting, the blood-pool lifetime of nanoparticles is partially determined by coating. Hydrophobic coatings tend to incur shorter half-lives.[29]

Iron nanoparticles are also coated for reasons of cytotoxicity; uncoated iron oxide nanoparticles have been shown to

increase the generation of reactive oxygen species (ROS),[30] reduce cellular proliferation,[31] and even induce cell death[30] though typically not at low concentrations.[32] Uncoated SPIOs have been shown to have up to a sixfold increase in cytotoxicity compared to dextran-coated iron nanoparticles.[30] The best characterized coating for iron nanoparticles to date has been dextran, owing perhaps to its early approval for human work, and early biological characterization.[33] Although dextran-coated USPIOs are safe at low concentrations, they have been shown to incur hemolysis, platelet aggregation, and increased immune system activity at high concentrations.[34]

Studies of novel coating types commonly compare new coatings to dextran coatings and often report enhancements in cellular uptake.[20,35,36] Even coated nanoparticles may incur varied biological effects in labeled cells. For example, ferucarbotran-coated SPIOs increased mesenchymal stem cell (MSC) proliferation, owing to iron nanoparticles peroxidase-like activity.[37] Investigations into biocompatibility of coatings can be at the cellular or at the system levels. For example, citrate-coated USPIOs have been shown to temporarily increase ROS in rat macrophages though without cytotoxic effects,[38] while cationic USPIOs apparently induced no microhemorrhage or thrombus, no inflammatory processes, and no effect on hepatic or renal enzymes.[26] Specialized coatings have also been used to more precisely label cells in vivo. The nanoparticle coating can itself be conjugated with molecules of interest. Experiments have been performed with Herceptin-dextran-coated SPIOs, which provided useful contrast in cancer lines expressing HER2/neu.[39] Similar work has been performed with folic acid-poly(ethylene glycol)-coated SPIOs, which provided contrast in tumors expressing folate receptors,[40] and with prostate-specific membrane antigen (PMSA), which bound to PMSA positive tumors.[41] A thorough review of coatings for iron nanoparticles has been written by Gupta and Gupta.[5]

Iron Pharmacokinetics

Upon entering the bloodstream, SPIOs are phagocytosed by the reticuloendothelial system (RES; or macrophage–monocyte system) that removes SPIOs by receptor-mediated endocytosis from the blood pool. These nanoparticles are typically taken up by macrophages and phagocytic cells in the liver, bone marrow, and spleen.

The lysosomal compartments of macrophages gradually degrade the iron nanoparticles,[42] with radioactive tracers showing that the iron is ultimately incorporated into the body's iron store.[43] The degradation rate of MPIOs is significantly slower than that of smaller nanoparticles; under some circumstances, these particles can be observed on MRI months later.[44] The biodegradation rate of these particles can be varied, depending on size and coating.[45]

Blood-pool half-life is dependent on several factors, including size, coating, dose, and charge. The half-lives of these nanoparticles are in the order of minutes[46] to hours.[47] The half-life dose dependence is relatively minimal, with clinical dose ranges having similar pharmacokinetic profiles. Smaller SPIOs tend to have longer half-lives.[23] Human blood-pool half-lives are significantly longer than those of small mammals. For example, ferumoxytol's half-life in humans is 24–36 hours, while in rats, it is 2–3 hours.[47] Hence, USPIO experiments in animals typically require significantly higher doses, often on the order of 10 times the human dose per kilogram of body weight.

Magnetic Characterization of Iron Oxides

The paramagnetism induces magnetic field inhomogeneities. There are reductions in T_1, T_2, and T_2^* relaxation rates, so that the accumulation of iron oxide leads to darkening (hypointensity) on T_2- or T_2^*-weighted MRI and brightening (hyperintensity) on T_1-weighted MRI.[1,2] These hypointensities are much larger than the volume occupied by the actual contrast agent particles, which is known as the blooming effect and is useful in increasing the visibility of the contrast agent (Fig. 1A and 1B). However, negative contrast agents interfere with visualizing the underlying anatomical structures, and they do not represent the true size of the lesion or labeled cells. The latter is problematic when imaging is being used to assess lesion sizes.

Quantifying the efficiency of MRI contrast agents allows us to assess whether they have sufficient relaxivity for magnetic resonance (MR) visualization. The relaxivity value (r_1, r_2, and r_2^*) reflects the ability of a contrast agent to change the relaxation rate ($R_1 = 1/T_1$, $R_2 = 1/T_2$, and $R_2^* = 1/T_2^*$) of water per concentration of contrast agent[48]:

$$\Delta R_1 = r_1 \cdot [Fe] \qquad \Delta R_2 = r_2 \cdot [Fe] \qquad \Delta R_2^* = r_2^* \cdot [Fe]$$

Relaxation rate changes linearly with the concentration of contrast agent over a wide concentration range (Fig. 2) and is sensitive to field strength. Relaxivity also depends on iron oxide configuration; nanorods have been shown to have significantly greater relaxivity.[49] Nanoparticles with some degree of ferrimagnetism also evidence much stronger relaxivity; this has been used to enable single-cell tracking.[7]

We show an example of measuring relaxivity using MC03F (Bangs Laboratories), FeREX, and Feridex, whose properties are summarized in Table 1. Different concentrations of the contrast agents were prepared in solution, and the solutions' R_2 and R_2^* were determined (Fig. 2). From T_2 and T_2^* maps, the relaxivity values r_2 or r_2^* were quantified (Table 2). While larger iron particles typically have a higher r_2 and r_2^* owing to a larger crystal domain,[50] we found here that MC03F, a micrometer-sized agent, had a smaller r_2^* than Feridex, matching with the results borne out by others,[51] possibly owing to its coating.[52] It is possible to detect micrometer-sized agents by MRI even when only a few nanoparticles are present.[53]

Overview of Ex Vivo Labeling of Cells

Ex vivo labeling involves cell labeling outside of a living body by culturing cells with iron oxide. Subsequently, these labeled

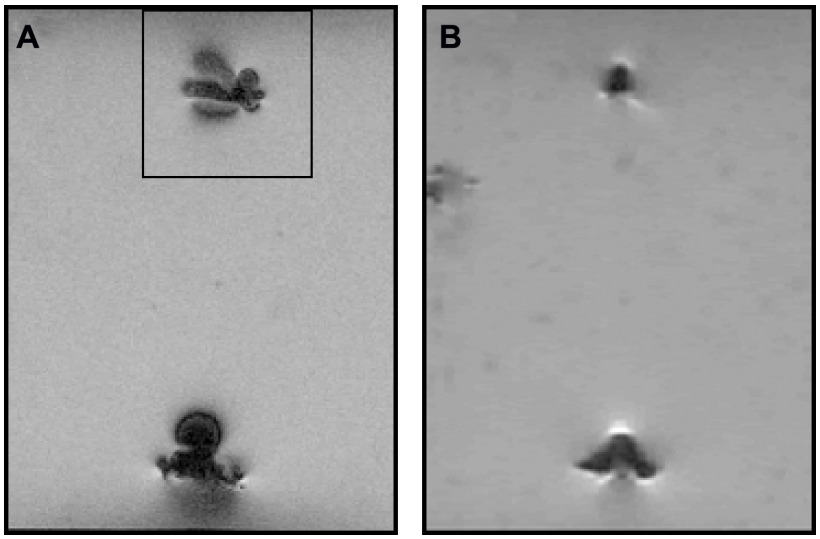

Figure 1. The magnetic field of an iron-labeled cell and its relation to the main magnetic field: the magnetic field is enhanced in the z direction and suppressed in the x direction. (**A**) FLASH image showing the bloom effect of iron in the MRI image. (**B**) RARE T_2-weighted image. (**A** and **B** have FeREX-labeled ESCs (4000 cells) at the top of the image and 5 μl of FeREX solution at the bottom. ESC labeling was accomplished by incubating a monolayer of ESCs (at 80% confluence) for 24 hours in 5% CO_2 at 37°C in a serum-free optimum medium with FeREX and Lipofectamine 2000 at a concentration of 25 μg Fe/mL).

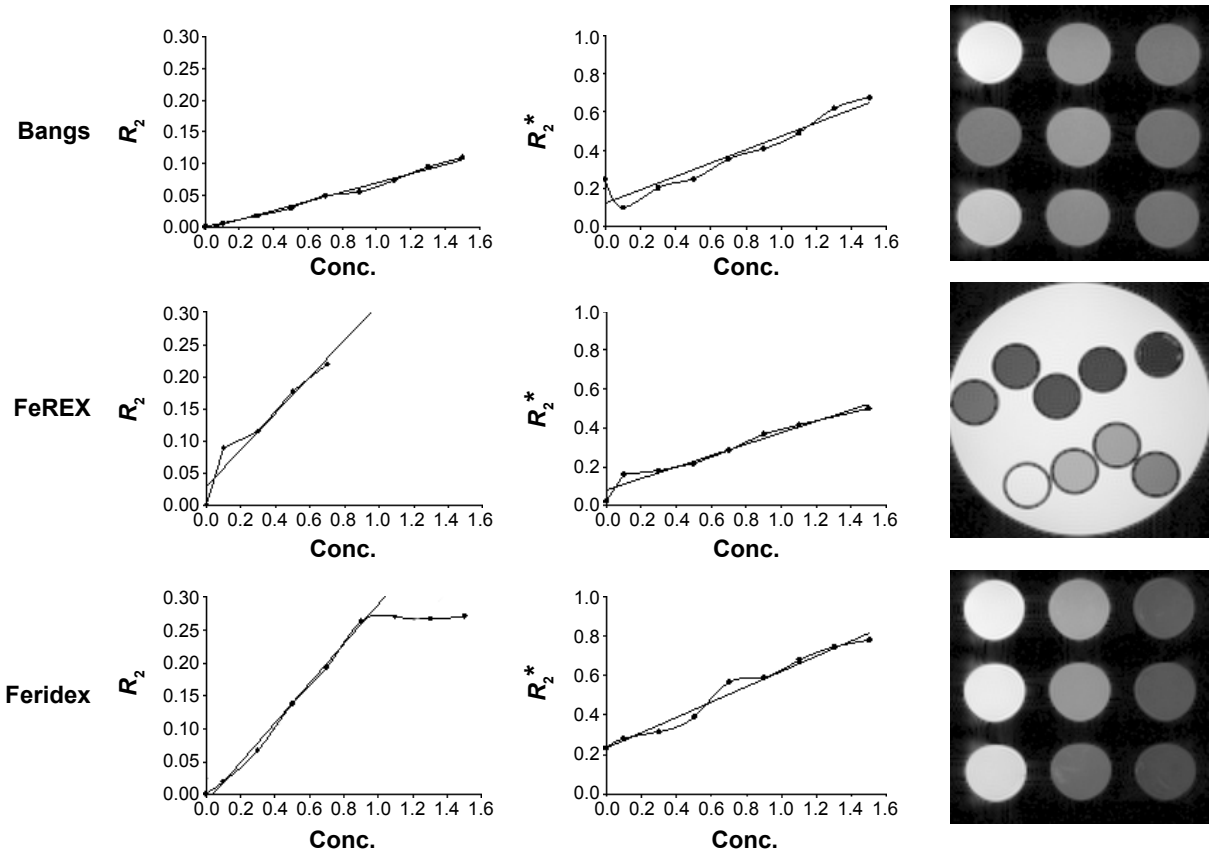

Figure 2. Relaxivity graphs for Bangs, FeREX, and Feridex particles and the corresponding MRI phantom images showing the different concentrations of dissolved contrast agents. R_2 and R_2* are in ms^{-1}, while concentration is in mM. Agents are in phosphate-buffer solution in small tubes that are then embedded in bigger containers of agarose to minimize imaging artifacts. The R_2 fit for Feridex ignores last three points because of nonlinearity. T_2 maps were obtained by a Carr Purcell Meiboom Gill sequence[177] with variable TEs (TR = 7500 ms, NA = 1, FOV = 3 × 3 cm^2, matrix = 128 × 128, 128 echo times, from 4 ms to 512 ms). T_2* maps were obtained with a multiple gradient echo sequence with variable TEs[178] (TR = 1500 ms, NA = 2, FOV = 3 × 3 cm^2, matrix = 128 × 128, with 7 echoes from 3 ms to 27 ms). Measurements of Feridex, FeREX, and Bangs are original measurements made in a Bruker 9.4 T MRI.

Table 1. A comparison between several common iron oxide contrast agents. PSC is polyglucose sorbitol carboxymethylether. Approval in some cases is not for imaging but for treatment of anemia (eg, ferumoxytol). Relaxivities of Feridex, Resovist, and Supravist at 3T are made in H_2O at 37°C by the study of Rohrer, Bauer, Mintorovitch, Requardt, and Weinmann.[174] Relaxivity of ferumoxytol[175] and FeREX[176] are more recent.

	FERIDEX	FeREX	BANGS (MC03F)	FERAHEME OR FERUMOXYTOL	RESOVIST	SUPRAVIST
Size	80–180 nm	50–150 nm	0.9 μm	17–31 nm	62 nm	25 nm
Coating	Dextran	Dextran	Styrene-DVB	PSC	Ferucarbotran	Ferucarbotran
Relaxivity 3T $mM^{-1}s^{-1*}$	$r_2 = 93 \pm 6$	$r_2 = 160 \pm 7$	$r_2 = 35.2$	$r_2 = 89$	$r_2 = 143 \pm 11$	$r_2 = 57 \pm 3$
Chemical formula	$FeO_{1.44}$	$FeO_{1.44}$	Fe_3O_4	$FeO_{1.49}$	Fe_3O_4	Fe_3O_4
Fluorescent properties	N/A	N/A	Flash red (660–690 nm)	N/A	N/A	N/A
Manufacturer	Advance Magnetics	Biopal Inc.	Bangs Labs	Takeda Inc.	Bayer	Bayer
Approval for Human	Approved	Approved	Not approved	Approved	Approved	Not approved

Note: *Mc03F has not had its r2 relaxivity measured at 3T but in NMR at 0.47T.

cells are injected or implanted into the organs of interest and imaged using MRI. Histology is used to confirm that iron is present in the loaded cell. It is possible for a labeled cell to die, releasing the iron; in such a situation, the iron could then be taken up by macrophages just as it would be in an in vivo labeling study.

Ex vivo labeling may have the advantage of increased specificity in the target cells. Cells not especially prone to endocytosis of iron nanoparticles, nonetheless, may be saturated in an environment where only the cells of interest may uptake the labeling compound without competition from incidental cells. Experiments examining the utility of a particular species of iron nanoparticle tend to emphasize the characterization of three traits: iron uptake in cultured cells, capacity to label daughter cells, and biological effects (e.g. apoptosis, nonviability of labelled cells, reduced protein production, etc.) of the nanoparticle.

Stem cells. Stem cells are an area of significant research interest as they may provide novel avenues for therapeutic treatments.[54] One appealing aspect of stem cell repair is their capacity to hone in on the site of injury. Thus, it is of interest to track the migration of stem cells to evaluate delivery efficiency without impairing the biological function of the stem cells. Labeling stem cells with iron oxide nanoparticles has grown into a popular technique in recent years, as with the correct biological coating or transfection agents, iron uptake can be accomplished with high efficacy.[55,56]

While iron nanoparticles, when used in labeling concentrations, do not totally inhibit stem cell function,[57] cellular viability does decrease in a dose-dependent manner at high concentrations in a variety of iron oxides.[20,58] While dextran-based coatings remain the most common coating for cellular labeling, citrate,[20] aminosilane,[58] and unfractionated heparin[36] coatings have been shown to improve stem cell uptake of iron nanoparticles. Conjugation with transfection agents, such as the HIV tat peptide, has yielded labeling rates of up to 10–30 pg Fe/cell, allowing for single-cell tracking of stem cells.[59]

While it is common to track injected stem cells via iron oxide labeling MRI, MRI does not distinguish between iron encapsulated within a surviving stem cell and iron recovered from apoptotic cells by macrophages. Histology has shown that MR signal from labeled and transplanted cells persists after cell death owing to tissue-bound macrophages.[60] This highlights the necessity of some external measure of validation (usually histology) to confirm that the cells labeled are the ones still being tracked.

A key aspect of stem cells is their proliferative ability. This may make maintaining the iron oxide label over multiple generations challenging.[44] Although this may not be a concern for stem cells that remain fixed while proliferating, it can make migrating stem cells challenging to track. One study that examined neuroblast migration along with the rostral migration stream to the olfactory bulb used MPIOs for their biological longevity and ability to label even with only a few particles.[44] MPIOs may prove ideal for long-term studies of stem cells, especially with MPIOs detectable with only a single particle.[61]

A study done by Taha et al[62] labeled embryonic stem cells (ESCs) using FeREX. The labeled ESCs were imaged

Table 2. The relaxivity values of the Feridex, FeREX, and Bangs MC03F contrast agents. Measurements are as described in Figure 2.

	FERIDEX	FeREX	BANGS (MC03F)
Relaxivity ($mM^{-1}s^{-1}$) at 9.4T	$r_2 = 307.5 \pm 12.9$	$r_2 = 283.6 \pm 44.1$	$r_2 = 72.1 \pm 2.6$
	$r_2^* = 389.4 \pm 22.9$	$r_2^* = 293.7 \pm 25.6$	$r_2^* = 350.3 \pm 40$

using fast low angle shot (FLASH) and rapid acquisition with relaxation enhancement (RARE) T_2 sequences. In MRI, the 4000 FeREX-labeled ESCs were detectable, appearing as a hypointense area with susceptibility artifacts surrounding it in FLASH and RARE T_2 sequences (Fig. 1B and 1C). This was confirmed with Prussian blue (PB) for histology, which showed that iron is inside the cells (Fig. 3).

Regenerative therapies using MSCs have been proposed for bone and cartilage repair. The exact role that MSCs play in repair is not fully characterized, so a noninvasive way to monitor stem cell migration would be useful. Histology and mass spectroscopy have shown that it is possible to label human MSCs without adversely impacting viability or proliferation.[63] Adipogenic, osteogenic, and chondrogenic differentiations of labeled cells were shown to be unaffected by gene expression.[63] However, MSC labeling approaches have seen impairment of chondrogenic differentiation with increasing dose of SPIO.[20] That said, the optimization of dosage and loading can minimize such impairment to negligible levels.[64,65] Human MSCs have been labeled and visualized by MRI in the collagen hydrogels that are now clinically used for cartilage repair.[63,66] MSCs have been used in a rabbit model of cartilage knee injury.[67] The injection of labeled MSCs caused signal decline in the defect, which reached a maximum at 4 weeks and returned to baseline after 12 weeks. Histology found labeled MSCs in the injury at 4 weeks, and none at 12 weeks, though they could be found outside the lesion. Animals treated with MSCs showed enhanced recovery; thus, these MRI results suggested that stem cells recruit native cells for repair.

Demyelination is common to many pathological conditions. Exogenously applied oligodendrocyte progenitors have been shown to support remyelination.[68] Oligodendrocyte progenitors are highly mobile and their movement correlates well with remyelination,[69] so iron labeling is also appropriate here. Bulte et al conjugated MION-46L with transferrin to label CG-4, an oligodendrocyte progenitor.[70] The labeled CG-4 cells were grafted into myelin-deficient rat spinal cords, and showed significant migration along the spine in MRI.[70] Regions of stem cell enhancement correlated strongly with new myelin formation. Improved neural progenitor labeling techniques have since been exactingly described.[71]

It may even be possible to use magnetic labeling to direct the delivery of stem cells in vivo. Magnetically labeled cells migrate toward magnets in culture through a phenomenon known as magnetophoresis.[72–74] One study injected labeled MSCs intravenously into rats and placed magnets over the livers of a subset of them. Those with magnetic direction had increased stem cell delivery to their livers, which corresponded to MR signal reductions.[72] Over the course of 30 days, MR enhancement faded, yet the MSCs remained fixed. Morphology of iron-labeled cells suggested that they were not simply Kupffer cells but appeared instead to be hepatocytes, perhaps originating as the injected MSCs.

Red blood cells. Contrast agents often clear from the blood within minutes to hours, but in some studies, it is desirable to have an agent that will remain circulating in the blood for days to weeks. A common role of MRI contrast agents is enhancement of the vasculature both to produce angiograms and venograms[75,76] and to calculate cerebral blood volume (CBV) by saturating the blood pool with the contrast agent.[77–79] However, the biological lifetime of free iron oxides in the blood is usually rather low, typically far less than 24 hours,[80,81] and so to do repeated measurements one would need repeated injections.

One approach to overcome this limitation has been the encapsulation of USPIOs within red blood cells (RBCs), which have a biological half-life of 3 months. Half-lives of up to 20 days have been demonstrated with this technique.[82] A variety of USPIOs—including commercially available Resovist and Sineram and experimental USPIOS—have been tested for compatibility with this technique.[83] Silicon-coated agents tend to be poorly encapsulated, and citrate agents are unsuitable because of their tendency to adsorb to the cellular membrane, which triggers elimination by the RES.

RBCs tend not to spontaneously load SPIO.[84,85] One loading technique requires that the integrity of the RBC's cellular membrane be temporarily compromised by hypotonic swelling in the presence of USPIOs and, after sufficient uptake, be restored.[86] This technique relies on the formation of pores

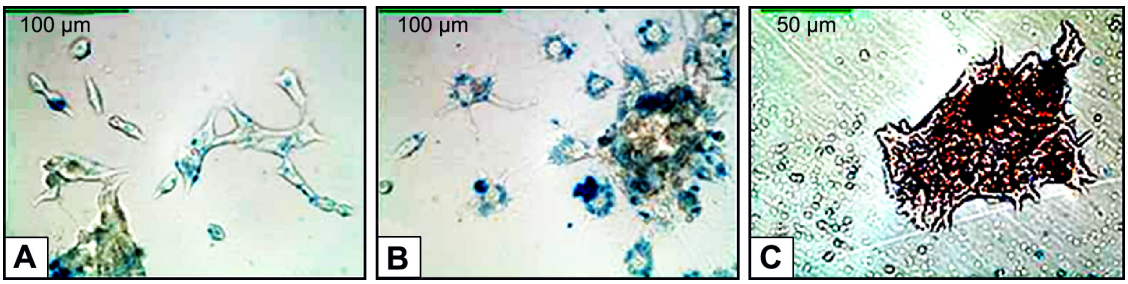

Figure 3. FeREX-labeled single layer of ESCs. (**A** & **B**) stained with PB; iron appears as blue spots. (**C**) PB-stained section and counterstained with nuclear fast red. Different aggregates of ESCs appear as red areas, and iron appears as blue spots. The cell labeling procedure here is the same as in Figure 1.

between 50 and 200 nm in diameter, which are sufficient to allow passage of the nanoparticles. When performed successfully, the majority of loaded RBCs are successfully recovered, and these RBCs have similar hemoglobin concentrations, full cellular integrity, and surface properties to unloaded RBCs.[84] The loading procedure tends to reduce cell volume, regardless of whether USPIOs are loaded.[86]

Research has shown that encapsulation slightly reduces the relaxivity of loaded USPIOs as compared to the bulk material in solution.[82] One explanation for this phenomenon is that the loading procedure favors the encapsulation of smaller nanoparticle crystals, which would reduce relaxivity slightly. Despite this slight reduction in relaxivity, loaded RBCs remain viable negative contrast agents that are highly compatible for use as a blood-pool enhancement or in magnetic particle imaging.

Overview of In Vivo Labeling of Cells

In vivo labeling involves injecting the contrast agent into an animal and having it taken up by cells. In vivo labeling of cells offers advantages compared to labeling cells in vitro and injecting them into the animal. One major advantage is that it is technically less challenging and less time-consuming, as one does not need to load the cells with USPIO in vitro. In addition, it offers a significant advantage in that it does not significantly introduce a foreign tissue into the animal, allowing one to monitor innate cell processes.

Macrophage–monocyte labeling. Labeling of macrophages has been shown to leave cells' macrophages viable, with labeled macrophages migrating to the sites of inflammation.[87] SPIOs have been shown to enhance the sites of inflammation. There are several proposed avenues for this enhancement.[88] Macrophages in the blood could uptake SPIOs before migrating to inflamed tissues. Alternatively, SPIOs could be transported by transcytosis across the epithelium at the sites of inflammation prior to endocytosis by macrophages already in situ. Another possibility is that leakage from the vasculature may take place because of vessel dilation, which results in SPIO deposition in the region of inflammation. Blood–brain barrier (BBB) breakdown has been shown to be accompanied by USPIO enhancement without immune cell involvement in stroke.[89] In cases without a leaking vasculature, it has been suggested that the dominant mechanism is endocytosis and subsequent migration of blood monocytes to the sites of inflammation. Mice treated with lipopolysaccharide (LPS), a substance that elicits a massive immune response, showed significant USPIO enhancement compared to the control group (Fig. 4).[90] However, when the monocytes were depleted with clodronate sulfate, the USPIO enhancement was abolished, indicating that iron endocytosis via blood monocytes is critical for USPIO enhancement of inflammation.[90] Regardless of mechanism, long half-life SPIOs appear to be an effective tool for demarking inflammation.

Nonlymphocyte labeling. While iron oxides tend to be taken up by the RES, other cell types may be targeted in vivo. Since MPIOs only require a few particles to be endocytosed, injection of MPIOs into the ventricles has been shown to be sufficient to label endogenous neural stem cells.[44] Tumor models have shown uptake of USPIOs into the intracellular compartment.[91] In nude mice (ie, without macrophages), it was shown that intravenous application of USPIO alone can enhance tumor cells, albeit variably.[92]

Targeted nanoparticles are those conjugated to some kind of targeting molecule.[10] The use of antibody coatings has enabled the in vivo labeling of antigen-expressing tumors.[39,93] USPIOs conjugated to Aβ1–42 peptides were used to detect amyloid plaque deposition, and could identify Alzheimer's disease mouse models. Injected MPIOs conjugated with antibodies for CD81 have been used to visualize atherosclerotic plaques,[94] and MPIOs conjugated to an antibody for the glycoprotein IIb/IIIa receptor of activated platelets have been used to visualize atherothrombosis[95] in mice. MPIOs may be of value for these targeted applications, as they clear from the blood, deliver a high dose of iron, and rarely leak through the

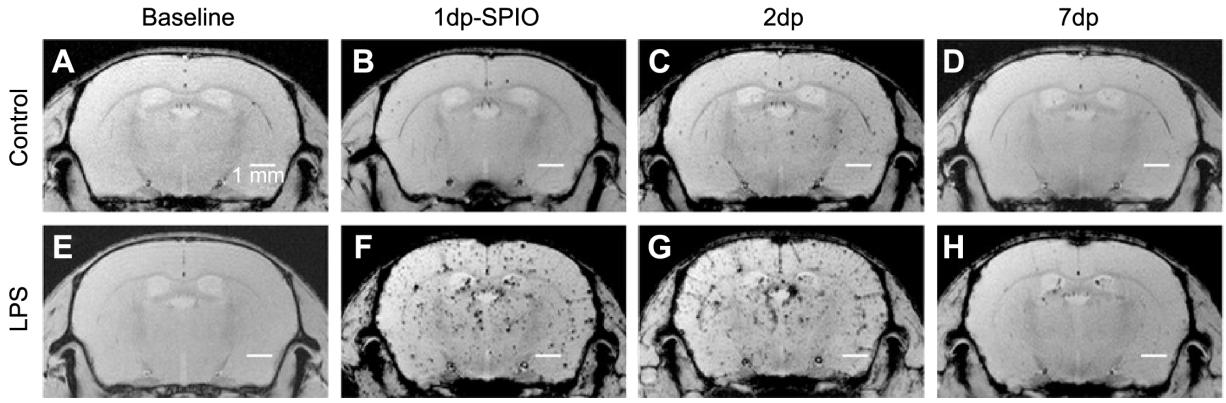

Figure 4. T_2*-weighted MRI showing LPS-induced SPIO enhancement: (**A**, **E**): before USPIO; (**B**, **F**): 1 day post SPIO; (**C**, **G**): 2 days post SPIO; (**D**, **H**): 7 days post SPIO. Upper row represents a control animal, and bottom row represents an animal injected with LPSs. Significant enhancement can be observed in the LPS group 1 and 2 days post SPIO injection. This enhancement resolves after 7 days. Figure adapted from Ref. 90.

vasculature. In a comparison between Gd and MPIO conjugated to a ligand for intercellular adhesion molecule-1 (ICAM-1), it is found that while both bound to ICAM-1 in vivo (as determined by histology), only the MPIO yielded significant MRI enhancement in vivo.[96] Angiogenesis has been visualized using both USPIO and MPIOs conjugated to arginine-glycine-aspartic acid (RGD), which binds to the sites of angiogenesis. It was found that the RGD-MPIOs had significantly greater specific binding and provided better contrast of regions with angiogenesis.[97]

Applications of Cell Tracking with Iron Nanoparticles

Ischemic stroke. Ischemic strokes are caused by a thrombus blocking off a major artery, reducing blood and oxygen delivery to the brain. The reduction of blood flow and oxygen causes acute tissue death (infarct). However, infarct volume continues to grow after the acute stage, suggesting that stroke-induced brain damage is not solely because of ischemia.[98] Blood-borne inflammatory cells infiltrate into the brain parenchyma after the initial ischemic insult; this is associated with the occurrence of postischemic neuronal loss.[98] Hence, monitoring inflammatory cell trafficking could be a useful prognostic marker in the subacute stages of ischemic stroke.

Several groups have shown that it is possible to noninvasively monitor blood monocyte migration by USPIO.[99,100] Using a rat photothrombotic model of ischemic stroke, it has been shown that there is USPIO enhancement in the infarct area 6 days postischemia.[99,100] Histology confirmed the colabeling of iron and proinflammatory phagocytes, indicating that brain inflammation during the subacute stage of stroke was detected by USPIO. Similar results have been obtained in a rat permanent middle cerebral artery occlusion model, with histology confirming USPIO colocalization with phagocytes on days 28 and 56.[101] One interesting trend was identified: inflamed regions without phagocytes (as imaged by USPIO) on day 7 tended to remain viable. This suggests that iron oxides may offer a noninvasive method of determining prognosis in stroke. Some caution is warranted, however. Stroke has been associated with BBB leakage (confirmed with Gd). Iron might leak through and subsequently be picked up by local macrophages, which could be confused with transiting invasive macropahges.[89,102]

Multiple sclerosis. Multiple sclerosis (MS) is a demyelinating, immune-mediated disease. Infiltrating macrophages are key players in demyelination[103] and typically tend to cluster in central nervous system (CNS) lesions typical of MS. Studying macrophage infiltration may yield insights into disease progression and treatment response.

Several studies have explored tracking macrophage infiltration with iron nanoparticles in the experimental autoimmune encephalomyelitis (EAE) model of MS in rodents. EAE is a well-characterized disease model that exhibits chronic inflammation and demyelination, similar to human MS.[104] Studies using iron nanoparticles in EAE and MS have been reviewed previously by Nathoo et al.[105] Studies tracking macrophage infiltration using iron nanoparticles in EAE models have demonstrated macrophage accumulation throughout the CNS, including in the spinal cord,[22,106] brainstem,[106,107] cerebellum,[106,107] and cortex.[108,109] It is worth noting that in cases where there is a high concentration of internalized iron, it is possible to visualize iron accumulation at the single-cell level,[22] making this a powerful tool for cell tracking. This is also relevant since studies have shown that iron deposition (corresponding to monocyte infiltration) occurs even in areas without BBB breakdown (as determined by Gd enhancement),[110–112] suggesting translocation via macrophages. Similar discrepancies have been observed in human MS studies (Fig. 5).[113–116] This suggests that not all regions of inflammation are associated with BBB breakdown. Thus, iron oxide nanoparticles allow for measurement of inflammation not possible with other MRI contrast agents.

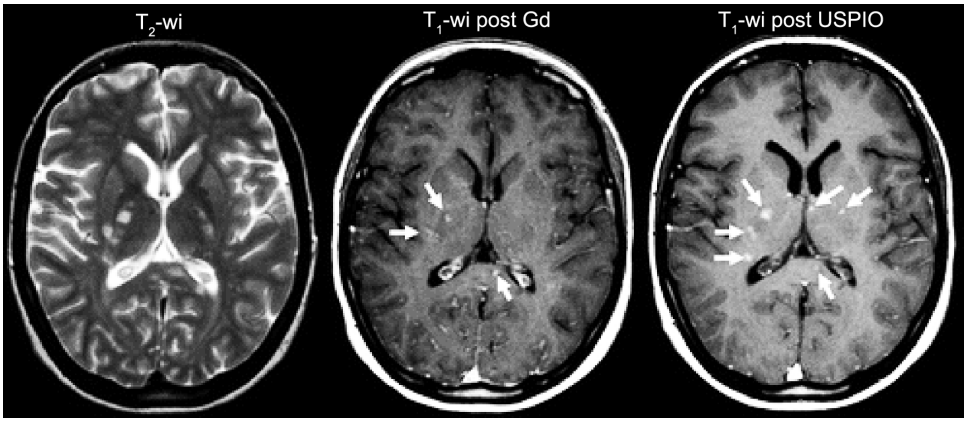

Figure 5. Discrepancies are present in lesion visualization between Gd-enhanced MRI (for BBB breakdown) and USPIO MRI (for macrophage accumulation). More lesions are observed with USPIO MRI (white arrows) as compared to Gd MRI (white arrows). Figure adapted and reproduced with permission from Ref. 115.

Labeling of monocytes with iron nanoparticles is also used to assess drug treatment response in MS and other conditions associated with inflammation. Studies using iron nanoparticles with MRI to assess drug treatment response have been reviewed by Nathoo et al.[117] In particular, the responses to disease-modifying therapies, such as natalizumab[118] and fingolimod,[119] have been tested using monocyte-labeled USPIOs with MRI. Treatment with natalizumab reduced monocyte infiltration into the CNS of EAE animals but did not prevent it completely,[118] whereas fingolimod treatment prevented the formation of lesions detected by USPIO in EAE animals.[119]

The response to lovastatin (a low-density lipoprotein lowering agent, thought to reduce cellular infiltration) has also been assessed in EAE animals using USPIOs.[110] Lovastatin suppresses monocyte infiltration, and it lessened the magnitude of the UPSIO darkening in treated EAE rats compared to untreated EAE rats. Less darkening by USPIOs correlated with improvements in EAE symptom scores. The results of these studies suggest that MRI with USPIOs can be used to track monocyte infiltration in inflammatory conditions and to assess response to treatments related to monocyte trafficking.

Cancer. Several approaches to visualizing tumors using USPIOs have been made. A common study design for cancer therapies entails the injection of a cancer line into a host animal. Some groups have labeled tumor cells, not hoping to visualize the immune cell response but simply to track the proliferation and spread of cancer in response to treatment. With recent advances in single-cell imaging,[120] some groups have managed to image single tumor cells in liver cancer,[121] though this has yet to be performed in a living animal.

Inflammatory immune cells, including tumor-associated macrophages (TAMs), affect cancer development. TAMs have been correlated with cancer prognosis. One group has explored GEH121333 and ferumoxytol, both USPIOs, to identify adenocarcinomas.[122] Persistent enhancement was observed from 24 to 72 hours later. Histology confirmed the internalization of USPIOs within TAMs.

In addition to their macrophage recruitment, tumors in the brain may also have associated microglia.[123] Fluorescently labeled USPIOs have been used to show that microglia internalize iron oxides at a high rate (above that of tumor cells and astrocytes).[124] In vitro work also showed that MR enhancement was dependent on immune cell count.[124] An in vivo rat study was conducted (16.74 mg Fe/kg delivered intravenous therapy with imaging preinjection and 24 hours postinjection) and showed significant tumor enhancement. Consistent with previous results,[125] the boundaries of tumors were enhanced, as phagocytic cells often form a barrier between tumor and brain.

Glioblastoma multiforme (GBM) is an aggressive CNS tumor with poor prognosis. There are some major applications of USPIOs in GBM. The first application is using multifunctional iron oxide nanoparticles to enhance the delivery of cytotoxic drugs to GBM. USPIO coatings can be modified to attach to tumor surface receptors, such as epidermal growth factor receptors, a receptor that is overexpressed in the majority of GBM tumors.[93] The modified iron oxide particles can then be attached to cytotoxic drugs, allowing more efficient delivery to tumor cells. It has been shown that treatment with a modified USPIOs tagged with cetuximab (a cytotoxic drug) resulted in significant antitumor effect compared to nontagged cetuximab, showing increased efficacy of cancer drug delivery to tumor cells.[93] Similar studies have been done, using modified USPIOs to deliver antitumor peptides, such as chlorotoxin.[126] The conjugation of therapeutic compounds to USPIOs is an interesting field with high potential. It opens up the possibility of noninvasively delivering a high-dose, cell-specific strategy to treat this aggressive cancer.

USPIOs are also used as blood-pool agents to differentiate pseudoprogression from true progression of tumors. Pseudoprogression is most commonly caused by radiation necrosis, which appears very similar to the recurrence of tumor on Gd-enhanced T1-weighted scans.[127] The current method of determining pseudoprogression is unreliable, as it does not have good correlation with survival.[127] Pseudoprogression can be determined by using dynamic contrast-enhanced MRI to measure CBV. Abnormalities with high CBV are suggestive of tumor, while abnormalities with normal or low CBV indicate pseudoprogression.[127,128]

Gd is the most common contrast agent used to measure CBV, but in GBM, the BBB is often broken, which results in contrast agents leaking into the tumor.[128] This yields an inaccurate CBV calculation and requires a leaking factor to be calculated in order to obtain the true CBV.[128] On the other hand, USPIOs, such as ferumoxytol, can act as blood-pool agents but do not exhibit contrast leakage even when the BBB is compromised.[129] Ferumoxytol has been shown to reliably differentiate pseudoprogression from cancer recurrence.[127,128] It has been shown that abnormal regions with a low CBV (suggestive of pseudoprogression), as calculated using ferumoxytol, is associated with significantly prolonged survival compared to abnormal regions with high CBV (true progression).[127,128] In addition, a leaking correction factor for CBV did not need to be calculated for ferumoxytol, unlike Gd.[128] Ferumoxytol can be a promising blood-pool agent in conditions where the BBB is compromised.

Immune therapy is establishing itself as a new method of treating cancer. The immune system is suppressed in many types of cancer, including GBM.[130,131] USPIOs can be a promising tool to label immune cells and assess the efficacy of such types of therapies. It has been shown that amphotericin B (AmpB) can activate innate immunity, suppress GBM, and prolong mice's life span.[132] AmpB increases the total number of circulating monocytes and the number of proinflammatory macrophages in the tumor.[132] By labeling monocytes with USPIOs, drug response of AmpB (ie, upregulation of blood monocytes and infiltration of monocytes into the tumor)

could possibly be detected even before there is any evidence of changes in tumor volume.

Iron oxide nanoparticles can also be used in DC-based vaccines to assess the efficacy of cancer immune therapy.[133] The success of DC vaccine therapy depends on the migration of vaccinated DCs to lymph nodes to activate T cells and elicit an antitumor response. Therefore, in vitro labeling of vaccinated DCs using USPIOs to track their location can be a very powerful tool to assess treatment response. USPIOs have been shown to leave DC viability largely unimpaired.[133] A dose-dependent lymph node signal drop has been shown to occur when using magnetically labeled DCs injected into the sites of inflammation, with histology confirming both iron and immune cells in the lymph nodes.[134] One group developed a magnetically labeled cancer vaccine, using a SPIO-labeled tumor mixed with Granulocyte macrophage colony stimulating factor (GM-CSF) secreting bystander cells.[6] This approach showed that signal decreases in lymph nodes three days postinjection, which coincided with the arrival of magnetically labeled DCs in the lymph nodes. These DCs were shown to induce the proliferation of T cells targeting factors expressed by the tumor cells.

Angiogenesis is critical to the development of tumors. RGD acts as a ligand to $\alpha_v\beta_3$ integrin, a marker for angiogenesis.[97] RGD-conjugated MPIOs (2.8 μm diameter) were first examined in vitro in both static and flow chamber cultures with human umbilical vein endothelial cells.[97] The MPIOs had significantly greater specific binding to the activated cells than control cells. Subsequent in vivo work found that RGD-conjugated MPIOs enhanced colorectal- and melanoma-derived tumors.[97] Histology confirmed that MPIOs were colocalized with neovessels. This suggests that targeted MPIOs may serve as a useful tool for tracking tumor growth and potentially as a platform for delivering drugs to the regions of angiogenesis.

Vascular disease (arteriovenous malformations, cerebral aneurysms, and aortic aneurysms). Iron oxide contrast agents have been used in vascular diseases, such as arteriovenous malformations (AVMs), cerebral aneurysms, and aortic aneurysms for various purposes. In the context of brain AVMs in humans, the USPIO agent ferumoxytol has been used as a blood-pool agent in combination with susceptibility-weighted MRI to help better delineate such vascular alterations in the forms of capillary telangiectasias and cavernomas.[135] With ferumoxytol sequences, 40 lesions were detected, while with pre- and postgadoteridol images, only 35 lesions were detected among the 19 patients in the study. The inclusion of ferumoxytol and susceptibility-weighted MRI enabled the visualization of tributary veins that were not apparent with pre- and postgadoteridol imaging with T_1-weighted MRI. A different study used ferumoxytol-enhanced MRI to highlight macrophages in brain AVMs in four patients. As one of the patients in the study underwent surgical resection of their AVM after imaging, staining of tissue for macrophages was compared with MRI findings; these appeared to be present in the same regions in the vascular wall.[136] The results from this small study are encouraging, but more studies are needed to compare ferumoxytol-enhanced MRI with the presence of macrophages in brain AVMs.

Iron oxide contrast agents have also been used in the setting of unruptured abdominal aortic aneurysms (AAAs) and cerebral aneurysms to assess macrophage infiltration in the vessel wall. AAAs are associated with inflammatory activity; thus, imaging such inflammation using iron oxide contrast agents to label macrophages is a possibility. One study used USPIOs to determine the rate of growth of AAAs. Those with asymptomatic aortic aneurysms ranging in size from 4 cm to 6.6 cm were imaged at 3T using T_2*-weighted MRI before and after the administration of USPIOs, where the change in T_2* value was correlated with histology for macrophages in the aneurysm tissue. Those with USPIO uptake in the vessel wall had a threefold higher growth rate compared to those that did not have such uptake.[137] This pilot study demonstrates the potential utility of imaging AAAs with iron oxide contrast agents, but more work is needed in the field.

Macrophages are also a significant component of cerebral aneurysms, lending them to being imaged with iron oxide contrast agents. In patients with unruptured cerebral aneurysms, MRI with ferumoxytol has been compared with tissue staining for macrophages (with CD68) and for the uptake of iron particles (with PB), with the finding being that ferumoxytol uptake seen with MRI is well correlated with the presence of macrophages in the aneurysm wall.[138] Furthermore, the optimal time between administration of ferumoxytol and subsequent imaging has also been compared, where more MRI signal changes were seen when there was a three-day delay in imaging postferumoxytol administration as compared to a one-day delay.[138] The same group conducted more research on the significance of early MRI changes with ferumoxytol administration (ie, 24 hours after administration)—mainly, they wanted to know if this suggests that the aneurysm is unstable. For this study, they investigated 30 unruptured aneurysms, of which 7 showed early uptake of ferumoxytol.[139] Of those seven, four were clipped soon after, while three were not, and of note, all three ruptured within 6 months. It is also worth noting that macrophages were similar in unruptured aneurysms with early uptake of ferumoxytol and ruptured aneurysms, suggesting that early uptake of ferumoxytol may be indicative of pending aneurysm rupture.[139] As the sample size for this study was quite small, it would be interesting to see if future studies come to the same conclusion as this one did. Imaging of cerebral aneurysms, with iron oxide contrast agents, has been reviewed more in depth by Levitt et al.[140]

Quantification with Iron Oxide Agents

Determination of iron oxide concentration in a region of interest is desirable for several reasons. The degree of cellular iron uptake can be used to probe cytotoxicity outcome.[141] If

quantification can be done in the magnet, it can yield CBV; in nondividing or slowly dividing cells, it can yield cell counts and can quantify iron biodistribution. If iron oxides are functionalized as part of a drug payload[11] or for use in hyperthermia,[27,142,143] quantification may aid understanding treatment efficacy.

Relaxivity is dependent on environmental factors that limit the areas in which relaxation rate measurements can be applied. One approach that has thus far only been applied in vitro has been the use of susceptibility imaging to obtain concentration. Susceptibility does not change much between encapsulated and free iron, making iron oxide concentration measurements feasible.[144] Relaxivity changes during encapsulation, with r_1 and r_2 reduced and r_2^* increased.[144–146] Then by combining relaxation time measurements and knowledge of concentration, intracellular and extracellular iron concentrations can be determined.[144] Unfortunately, this approach is sensitive to susceptibility effects, such as those induced by oxyhemoglobin and deoxyhemoglobin, though it may be useful as a nondestructive in vitro means of assessing labeling efficacy. In vivo quantification with this technique will face challenges requiring better modeling of other sources of susceptibility.

An approach that has seen more success in vivo is the use of electron paramagnetic resonance (EPR) spectroscopy. EPR spectroscopy has been used to assess in vitro iron oxide concentration where it was found to have a 91 ng Fe/mL lower limit of detection and 304 ng Fe/mL lower limit of quantification.[147] This was obtained for loading of the 35 nm USPIO Molday Ion Rhodamine B (MIRB) in RENA-luc (7 pg/cell) and B16F10-luc cells (10–13 pg/cell) at 9 GHz.[147] The same group subsequently injected mice with labeled renal[148] and breast cancer cells.[8] The renal cells lodged in the lungs and liver; EPR was, however, unable to track them in vivo beyond one day, owing to reduced sensitivity of their in vivo system.[148] With breast cancer, cell loading was sufficiently high to enable single-cell tracking using T_2^*-weighted imaging at 11.7 T.[8] Having first characterized the iron per cell in vitro, subsequent EPR measurements in ex vivo brains enabled iron concentration determination and hence cell counting (ignoring proliferative effects).[8] Beyond one day postinjection, however, the MIRB signal was lost owing to degradation and proliferation, and did not appear in their ex vivo EPR work.[8]

Apparent diffusion coefficient (ADC) can be changed in the presence of iron. In an in vivo Macaque study, this change in ADC disappears when bipolar pulses are used, allowing the estimation of ξ_{Fe}, a parameter estimating the ADC change because of iron.[149] This method showed sensitivity to regions of the brain known to endemically contain greater iron concentration and to USPIO injection.[149] Since iron is already present in the macaque brain and has been characterized by age and anatomy,[150] a linear mapping between ξ_{Fe} and [Fe] could be made.[149] However, the fit of this map was rather poor: $\xi_{Fe} = 0$ suggested a negative [Fe] of –371.5 μg/g of brain. The authors speculate that the relationship between the two parameters is not linear, and that further calibration will enable absolute quantification.

Quantification as a blood-pool contrast agent. A common use of contrast agents is in saturating the blood pool to perform angiography and venography[75,76] and derive vascular information, including blood volume (BV),[151] vessel diameter,[152,153] and water exchange.[154] Owing to iron oxide's blooming effect in T_2^* images, they are less sensitive to the microvasculature than T_2 images.[151] T_2 images may be used to map CBV sensitive to the microvasculature,[79] though T_2^* is more common for total CBV.[151] This difference in sensitivity has been exploited to determine differences in vessel diameter.[152]

Visualizing the blood via contrast agent yields angiographies and venographies. Iron oxides act as a negative contrast agent for T_2 and T_2^* images, and may be used in this capacity. Since T_2^* images are susceptible to blooming effects, T_2 images are better for visualizing microvasculature. Another option is to exploit SPIOs' positive contrast effects on T_1 images. However, attempts that visualize this with off-resonance imaging or imaging of local field inhomogeneities[155] were challenged by sensitivity and susceptibility artifacts.[156]

One approach to overcome these problems was the use of ultrashort time to echo (UTE) imaging sequences. The short time to echo means that dephasing because of T_2^* effects is minimal, and good quality T_1 images may be generated.[157] Using 3D UTE, Gharagouzloo et al[15] were able to simultaneously make high fidelity quantitative ferumoxytol concentration measurements in vitro (3.0% mean error) and in vivo in mice (7.1% mean error). This enabled the determination of ferumoxytol blood-pool half-life.[15] Blood-pool half-life measurements were also made by multiple-echo (0.1, 0.8, and 1.6 ms) 3D UTE for four different coatings, such as citric, etidronic, malic, and tartaric acids, albeit without determining absolute concentration.[46] This approach could be adapted to determine absolute concentration if r_2^* were known for these nanoparticles.[46]

When performing angiography and interrogating the vasculature, it is sometimes of use to examine other properties of the vasculature. T_1, T_2, and T_2^* are complementary in this effort, with each providing the means (when coupled with a contrast agent) to quantify different vascular properties.[156] An imaging sequence has been designed that quantified vascular properties, such as water exchange index (via T_1), BV (via ΔR_2), and vessel caliber index (via ΔR_2^*).[156] The T1 images were generated via UTE, while the T2 images were a standard multislice multiecho sequence and the T2* images a multiple gradient echo sequence.[156] For this, they employed 29 mg/kg of long half-life dextran-coated USPIO (hydrostatic diameter of 20 ± 5 nm).[156] Their in vivo results were self-consistent in mice, with both hemispheres presenting similar quantities.[156] Measurement of CBV and mean vessel size have also been reported with iron oxide-enhanced UTE.[158] It thus appears possible to exploit the dual-contrast enhancement offered by SPIOs and thoroughly examine vascular properties.

Designing Studies using Iron Contrast Agents

A lab intent on employing iron nanoparticles will typically want to perform several steps of validation before attempting a labeling study. Typically, validation will begin with in vitro work. An illustrative paper of this process was published by Engberink et al, in which human leukocytes were loaded with SPIOs and USPIOs.[159] This paper incorporated four common validation steps as follows: i) T_2 measurements of solutions at different concentrations of iron were made; ii) cell loading was studied histologically via the colocalization of nuclear fast red and PB staining; iii) MRI signal was examined via an nuclear magnetic resonance phantom consisting of cells in agar and was used to determine optimal culturing and loading parameters; and iv) cell viability was established via measurements of cellular migration, proliferation, and production of extracellular factors (IL-1 and IL-6 in this case). This validation could then be followed by a study using these labeled cells. Indeed, the authors of this article followed this work with an immune cell study ex vivo.[22]

Limitations

Even coated nanoparticles have subtle immunological effects[34] and can affect cellular proliferation (negatively[58] or positively[37]), and nanoparticles can be toxic to certain cells at high concentrations.[31] While cytotoxicity is typically dose dependent, low-dose labeling decreases MRI visibility. For this reason, developing high relaxivity nanoparticles and employing higher field MRIs is useful, so that less iron is required to obtain the same contrast. Exploiting ferrimagnetism,[7] nonspherical geometries,[49] nanocluster,[160] or even simply using MPIOs[53,161,162] can meet these requirements. Avoiding the use of transfection agents and still obtaining good labeling are often possible[163] and may prove less toxic. While there are iron oxides that appear to be largely safe at imaging doses,[164] some adverse systemic effects have been reported in human trials.[165] The Food and Drug Administration now warns that ferumoxytol may pose a fatal allergic reaction risk.[166]

One challenge with using iron oxides is that their relaxivity changes depending on the environment they find themselves situated in. This poses challenges to their quantification.[144] Quantification also often depends on assumptions of intravascularity[15,156] or is sensitive to dilution.[8,147,148] Cell labeling quality is often degraded as iron oxide becomes dilute by proliferation[8] or by lysosomal action, though MPIOs are more resilient to these effects.[44,146,161]

Typical imaging schemes with iron oxides use iron as a negative contrast agent. To track iron, two images, such as a precontrast and a postcontrast image, are often used.[167] Some positive contrasts (white marker techniques) do exist, but they deposit more energy and are more complicated.[167] T_1 shortening may be employed, but is complicated by rapid T_2* decay.[46] This may be addressed with UTE imaging, but this is a challenging technique.[46,158] Most MRI images ^{1}H, but other half-integer spin nuclei can also be imaged. One such technology is ^{19}F MRI that is a positive contrast approach with high signal to noise, as ^{19}F does not naturally occur in the human body,[168] and has been used for cell tracking.[169,170] Other half-spin nuclei are typically weaker but can be hyperpolarized to generate signals on the order of 10^4 times stronger.[171] Cell tracking has been accomplished with ^{129}Xe,[172] and cancer imaging with ^{13}C.[173]

It is difficult to be certain about which cells nanoparticles find themselves in or whether they are in the cellular compartment at all. For example, when studying iron oxides situated in the brain, infiltrating macrophages may be credited with iron oxide presence,[110,119] or BBB leakage may be to blame.[89] The presence of iron in a region does not guarantee that the cells they originally labeled are still alive.[60] While histology often shows that iron oxides are localized within immune cells, noninvasively determining whether these are microglia or invasive macrophages remains difficult.[101,124]

Conclusion

Iron nanoparticles are a versatile tool for cell tracking and targeting cells for imaging. They may be introduced into the body where they provide contrast enhancement associated with macrophages and monocytes. Iron particles enable imaging of the liver, lymph nodes, spleen, and sites of inflammation. They may be introduced to a population of cells ex vivo, which may be tracked upon transplantation into the body. The diversity of available coatings and sizes for iron nanoparticles grants tremendous flexibility for cell and tissue targeting via conjugation with histological agents, antibodies, and transfection agents. The use of iron-based contrast agents for both preclinical and patient studies is on the rise and will be certain to provide novel information in the future.

Author Contributions

Conceived and designed the experiments: MT. Analysed the data: MT, DJK. Wrote the first draft of the manuscript: DJK, MT, RY, NN. Contributed to writing of the manuscript: DJK, MT, RY, NN, JFD. Jointly developed the structure and arguments for the paper: DJK, MT, RY, NN, JFD. Made critical revisions and approved final version: DJK, MT, RY, NN, JFD. All authors reviewed and approved of the final manuscript.

REFERENCES

1. Stoll G, Bendszus M. New approaches to neuroimaging of central nervous system inflammation. *Curr Opin Neurol*. 2010;23(3):282–286.
2. Reimer P, Müller M, Marx C, et al. T1 effects of a bolus-injectable superparamagnetic iron oxide, SH U 555 A: dependence on field strength and plasma concentration—preliminary clinical experience with dynamic T1-weighted M R imaging. *Radiology*. 1998;209(3):831–836.
3. Bulte JW, Duncan ID, Frank JA. In vivo magnetic resonance tracking of magnetically labeled cells after transplantation. *J Cereb Blood Flow Metab*. 2002;22(8):899–907.
4. Hawrylak N, Ghosh P, Broadus J, Schlueter C, Greenough WT, Lauterbur PC. Nuclear magnetic resonance (NMR) imaging of iron oxide-labeled neural transplants. *Exp Neurol*. 1993;121(2):181–192.
5. Gupta AK, Gupta M. Synthesis and surface engineering of iron oxide nanoparticles for biomedical applications. *Biomaterials*. 2005;26(18):3995–4021.
6. Long CM, van Laarhoven HWM, Bulte JWM, Levitsky HI. Magnetovaccination as a novel method to assess and quantify dendritic cell tumor antigen capture and delivery to lymph nodes. *Cancer Res*. 2009;69(7):3180–3187.

7. Lee N, Kim H, Choi SH, et al. Magnetosome-like ferrimagnetic iron oxide nanocubes for highly sensitive MRI of single cells and transplanted pancreatic islets. *Proc Natl Acad Sci U S A*. 2011;108(7):2662–2667.
8. Danhier P, Magat J, Levêque P, et al. In vivo visualization and ex vivo quantification of murine breast cancer cells in the mouse brain using MRI cell tracking and electron paramagnetic resonance. *NMR Biomed*. 2015;28(3):367–375.
9. Shapiro EM, Sharer K, Skrtic S, Koretsky AP. In vivo detection of single cells by MRI. *Magn Reson Med*. 2006;55(2):242–249.
10. Gauberti M, Montagne A, Quenault A, Vivien D. Molecular magnetic resonance imaging of brain–immune interactions. *Front Cell Neurosci*. 2014;8:389.
11. Quinto CA, Mohindra P, Tong S, Bao G. Multifunctional superparamagnetic iron oxide nanoparticles for combined chemotherapy and hyperthermia cancer treatment. *Nanoscale*. 2015;7(29):12728–12736.
12. El-Hammadi MM, Arias JL. Iron oxide-based multifunctional nanoparticulate systems for biomedical applications: a patent review (2008—present). *Expert Opin Ther Pat*. 2015;25(6):691–709.
13. Neuwelt A, Sidhu N, Hu C-AA, Mlady G, Eberhardt SC, Sillerud LO. Iron-based superparamagnetic nanoparticle contrast agents for MRI of infection and inflammation. *Am J Roentgenol*. 2015;204(3):W302–W313.
14. Sharifi S, Seyednejad H, Laurent S, Atyabi F, Saei AA, Mahmoudi M. Superparamagnetic iron oxide nanoparticles for in vivo molecular and cellular imaging [Published ahead of print (Apr 2015)]. *Contrast Media Mol Imaging*. 2015. doi: 10.1002/cmmi.1638.
15. Gharagouzloo CA, McMahon PN, Sridhar S. Quantitative contrast-enhanced MRI with superparamagnetic nanoparticles using ultrashort time-to-echo pulse sequences. *Magn Reson Med*. 2014;74(2):431–441.
16. Salunkhe A, Khot V, Pawar S. Magnetic hyperthermia with magnetic nanoparticles: a status review. *Curr Top Med Chem*. 2014;14(5):572–594.
17. Charles S, Popplewell J. Progress in the development of ferromagnetic liquids. *IEEE Trans Magn*. 1980;16(2):172–177.
18. Hunter R. *Colloid Science: Zeta Potential in Colloid Science: Principles and Applications*. London: Academic Press; 1981.
19. Zhang Y, Yang M, Portney NG, et al. Zeta potential: a surface electrical characteristic to probe the interaction of nanoparticles with normal and cancer human breast epithelial cells. *Biomed Microdevices*. 2008;10(2):321–328.
20. Andreas K, Georgieva R, Ladwig M, et al. Highly efficient magnetic stem cell labeling with citrate-coated superparamagnetic iron oxide nanoparticles for MRI tracking. *Biomaterials*. 2012;33(18):4515–4525.
21. Bulte JWM, Kraitchman DL. Iron oxide MR contrast agents for molecular and cellular imaging. *NMR Biomed*. 2004;17(7):484–499.
22. Engberink RD, van der Pol SM, Walczak P, et al. Magnetic resonance imaging of monocytes labeled with ultrasmall superparamagnetic particles of iron oxide using magnetoelectroporation in an animal model of multiple sclerosis. *Mol Imaging*. 2010;9(5):268–277.
23. Saito S, Tsugeno M, Koto D, et al. Impact of surface coating and particle size on the uptake of small and ultrasmall superparamagnetic iron oxide nanoparticles by macrophages. *Int J Nanomed*. 2012;7:5415–5421.
24. Calero M, Gutiérrez L, Salas G, et al. Efficient and safe internalization of magnetic iron oxide nanoparticles: two fundamental requirements for biomedical applications. *Nanomedicine*. 2014;10(4):733–743.
25. Lewandowska-Łańcucka J, Staszewska M, Szuwarzyński M, et al. Synthesis and characterization of the superparamagnetic iron oxide nanoparticles modified with cationic chitosan and coated with silica shell. *J Alloys Comp*. 2014;586:45–51.
26. Uchiyama MK, Toma SH, de Paula Rodrigues SF, et al. Ultrasmall cationic superparamagnetic iron oxide nanoparticles as nontoxic and efficient MRI contrast agent and magnetic-targeting tool. *Int J Nanomedicine*. 2015;10:4731–4746.
27. Bae KH, Park M, Do MJ, et al. Chitosan oligosaccharide-stabilized ferrimagnetic iron oxide nanocubes for magnetically modulated cancer hyperthermia. *ACS Nano*. 2012;6(6):5266–5273.
28. Wen X, Wang Y, Zhang F, et al. In vivo monitoring of neural stem cells after transplantation in acute cerebral infarction with dual-modal MR imaging and optical imaging. *Biomaterials*. 2014;35(16):4627–4635.
29. Gaur U, Sahoo SK, De TK, Ghosh PC, Maitra A, Ghosh PK. Biodistribution of fluoresceinated dextran using novel nanoparticles evading reticuloendothelial system. *Int J Pharm*. 2000;202(1–2):1–10.
30. Yu M, Huang S, Yu KJ, Clyne AM. Dextran and polymer polyethylene glycol (PEG) coating reduce both 5 and 30 nm iron oxide nanoparticle cytotoxicity in 2D and 3D cell culture. *Int J Mol Sci*. 2012;13(5):5554–5570.
31. Singh N, Jenkins GJS, Asadi R, Doak SH. Potential toxicity of superparamagnetic iron oxide nanoparticles (SPION). *Nano Rev*. 2010;1:5358.
32. Hussain SM, Hess KL, Gearhart JM, Geiss KT, Schlager JJ. In vitro toxicity of nanoparticles in BRL 3A rat liver cells. *Toxicol In Vitro*. 2005;19(7):975–983.
33. Bengele HH, Palmacci S, Rogers J, Jung CW, Crenshaw J, Josphson L. Biodistribution of an ultrasmall superparamagnetic iron oxide colloid, BMS 180549, by different routes of administration. *Magn Reson Imaging*. 1994;12(3):433–442.
34. Easo SL, Mohanan PV. In vitro hematological and in vivo immunotoxicity assessment of dextran stabilized iron oxide nanoparticles. *Colloids Surf B Biointerfaces*. 2015;134:122–130.
35. Berry CC, Wells S, Charles S, Curtis ASG. Dextran and albumin derivatised iron oxide nanoparticles: influence on fibroblasts in vitro. *Biomaterials*. 2003;24(25):4551–4557.
36. Lee JH, Jung MJ, Hwang YH, et al. Heparin-coated superparamagnetic iron oxide for in vivo MR imaging of human MSCs. *Biomaterials*. 2012;33(19):4861–4871.
37. Huang DM, Hsiao JK, Chen YC, et al. The promotion of human mesenchymal stem cell proliferation by superparamagnetic iron oxide nanoparticles. *Biomaterials*. 2009;30(22):3645–3651.
38. Stroh A, Zimmer C, Gutzeit C, et al. Iron oxide particles for molecular magnetic resonance imaging cause transient oxidative stress in rat macrophages. *Free Radic Biol Med*. 2004;36(8):976–984.
39. Chen TJ, Cheng TH, Chen CY, et al. Targeted herceptin–dextran iron oxide nanoparticles for noninvasive imaging of HER2/neu receptors using MRI. *J Biol Inorg Chem*. 2009;14(2):253–260.
40. Chen TJ, Cheng TH, Hung YC, Lin KT, Liu GC, Wang YM. Targeted folic acid-PEG nanoparticles for noninvasive imaging of folate receptor by MRI. *J Biomed Mater Res A*. 2008;87(1):165–175.
41. Bates D, Abraham S, Campbell M, Zehbe I, Curiel L. Development and characterization of an antibody-labeled super-paramagnetic iron oxide contrast agent targeting prostate cancer cells for magnetic resonance imaging. *PLoS One*. 2014;9(5):e97220.
42. Schulze E, Ferrucci JT Jr, Poss K, Lapointe L, Bogdanova A, Weissleder R. Cellular uptake and trafficking of a prototypical magnetic iron oxide label in vitro. *Invest Radiol*. 1995;30(10):604–610.
43. Weissleder R, Elizondo G, Wittenberg J, Rabito CA, Bengele HH, Josephson L. Ultrasmall superparamagnetic iron oxide: characterization of a new class of contrast agents for MR imaging. *Radiology*. 1990;175(2):489–493.
44. Roose D, Leroux F, De Vocht N, et al. Multimodal imaging of micron-sized iron oxide particles following in vitro and in vivo uptake by stem cells: down to the nanometer scale. *Contrast Media Mol Imaging*. 2014;9(6):400–408.
45. Shapiro EM. Biodegradable, polymer encapsulated, metal oxide particles for MRI-based cell tracking. *Magn Reson Med*. 2015;73(1):376–389.
46. Scharlach C, Warmuth C, Schellenberger E. Determination of blood circulation times of superparamagnetic iron oxide nanoparticles by T2* relaxometry using ultrashort echo time (UTE) MRI [Published ahead of print (June 2015)]. *Magnetic Resonance Imaging*. 2015. doi:10.1016/j.mri.2015.06.017
47. Corot C, Robert P, Idée J-M, Port M. Recent advances in iron oxide nanocrystal technology for medical imaging. *Adv Drug Deliv Rev*. 2006;58(14):1471–1504.
48. Hornak JP. The Basics of MRI. Interactive Learning Software, Henietta, NY; 2008: https://www.cis.rit.edu/htbooks/mri/ Accessed by May 10, 2015, chapter 8.
49. Mohapatra J, Mitra A, Tyagi H, Bahadur D, Aslam M. Iron oxide nanorods as high-performance magnetic resonance imaging contrast agents. *Nanoscale*. 2015;7(20):9174–9184.
50. Jun YW, Huh YM, Choi JS, et al. Nanoscale size effect of magnetic nanocrystals and their utilization for cancer diagnosis via magnetic resonance imaging. *J Am Chem Soc*. 2005;127(16):5732–5733.
51. Hinds KA, Hill JM, Shapiro EM, et al. Highly efficient endosomal labeling of progenitor and stem cells with large magnetic particles allows magnetic resonance imaging of single cells. *Blood*. 2003;102(3):867–872.
52. Duan H, Kuang M, Wang X, Wang YA, Mao H, Nie S. Reexamining the effects of particle size and surface chemistry on the magnetic properties of iron oxide nanocrystals: new insights into spin disorder and proton relaxivity. *J Phys Chem C*. 2008;112(22):8127–8131.
53. Leder A, Raschzok N, Schmidt C, et al. Micron-sized iron oxide-containing particles for microRNA-targeted manipulation and MRI-based tracking of transplanted cells. *Biomaterials*. 2015;51:129–137.
54. Bianco P, Riminucci M, Gronthos S, Robey PG. Bone marrow stromal stem cells: nature, biology, and potential applications. *Stem Cells*. 2001;19(3):180–192.
55. Frank JA, Zywicke H, Jordan EK, et al. Magnetic intracellular labeling of mammalian cells by combining (FDA-approved) superparamagnetic iron oxide MR contrast agents and commonly used transfection agents. *Acad Radiol*. 2002;9(suppl 2):S484–S487.
56. Frank JA, Miller BR, Arbab AS, et al. Clinically applicable labeling of mammalian and stem cells by combining superparamagnetic iron oxides and transfection agents. *Radiology*. 2003;228(2):480–487.
57. Saldanha KJ, Doan RP, Ainslie KM, Desai TA, Majumdar S. Micrometer-sized iron oxide particle labeling of mesenchymal stem cells for magnetic resonance imaging based monitoring of cartilage tissue engineering. *Magn Reson Imaging*. 2011;29(1):40–49.
58. Zhu XM, Wang YX, Leung KC, et al. Enhanced cellular uptake of aminosilane-coated superparamagnetic iron oxide nanoparticles in mammalian cell lines. *Int J Nanomedicine*. 2012;7:953–964.

59. Lewin M, Carlesso N, Tung CH, et al. Tat peptide-derivatized magnetic nanoparticles allow in vivo tracking and recovery of progenitor cells. *Nat Biotech*. 2000;18(4):410–414.
60. Terrovitis J, Stuber M, Youssef A, et al. Magnetic resonance imaging overestimates ferumoxide-labeled stem cell survival after transplantation in the heart. *Circulation*. 2008;117(12):1555–1562.
61. Shapiro EM, Skrtic S, Sharer K, Hill JM, Dunbar CE, Koretsky AP. MRI detection of single particles for cellular imaging. *Proc Natl Acad Sci U S A*. 2004;101(30): 10901–10906.
62. Taha MA, Roman K, Rancourt DE, Matyas JR, Dunn JF. Tracking iron labeled stem cells in bone injury model using MRI. In: 23rd Annual ISMRM. 2015. Toronto, ON.
63. Heymer A, Haddad D, Weber M, et al. Iron oxide labelling of human mesenchymal stem cells in collagen hydrogels for articular cartilage repair. *Biomaterials*. 2008;29(10):1473–1483.
64. Schulze F, Dienelt A, Geissler S, et al. Amino-polyvinyl alcohol coated superparamagnetic iron oxide nanoparticles are suitable for monitoring of human mesenchymal stromal cells in vivo. *Small*. 2014;10(21):4340–4351.
65. Eamegdool SS, Weible MW, Pham BT, Hawkett BS, Grieve SM, Chan-ling T. Ultrasmall superparamagnetic iron oxide nanoparticle prelabelling of human neural precursor cells. *Biomaterials*. 2014;35(21):5549–5564.
66. Hesse E, Hefferan TE, Tarara JE, et al. Collagen type I hydrogel allows migration, proliferation, and osteogenic differentiation of rat bone marrow stromal cells. *J Biomed Mater Res A*. 2010;94(2):442–449.
67. Jing XH, Yang L, Duan XJ, et al. In vivo MR imaging tracking of magnetic iron oxide nanoparticle labeled, engineered, autologous bone marrow mesenchymal stem cells following intra-articular injection. *Joint Bone Spine*. 2008;75(4):432–438.
68. Duncan ID, Milward EA. Glial cell transplants: experimental therapies of myelin diseases. *Brain Pathol*. 1995;5(3):301–310.
69. Warrington AE, Barbarese E, Pfeiffer SE. Differential myelinogenic capacity of specific developmental stages of the oligodendrocyte lineage upon transplantation into hypomyelinating hosts. *J Neurosci Res*. 1993;34(1):1–13.
70. Bulte JW, Zhang S, van Gelderen P, et al. Neurotransplantation of magnetically labeled oligodendrocyte progenitors: magnetic resonance tracking of cell migration and myelination. *Proc Natl Acad Sci U S A*. 1999;96(26):15256–15261.
71. Sart S, Bejarano F, Yan Y, Grant S, Li Y. Labeling Pluripotent Stem Cell-Derived Neural Progenitors with Iron Oxide Particles for Magnetic Resonance Imaging. In: Turksen K, ed. *Stem Cells and Good Manufacturing Practices*. Vol 1283: Springer New York; 2015:43–52.
72. Arbab AS, Jordan EK, Wilson LB, Yocum GT, Lewis BK, Frank JA. In vivo trafficking and targeted delivery of magnetically labeled stem cells. *Hum Gene Ther*. 2004;15(4):351–360.
73. Kolosnjaj-Tabi J, Wilhelm C, Clement O, Gazeau F. Cell labeling with magnetic nanoparticles: opportunity for magnetic cell imaging and cell manipulation. *J Nanobiotechnology*. 2014;11(suppl 1):S7.
74. Wilhelm C, Gazeau F, Bacri JC. Magnetophoresis and ferromagnetic resonance of magnetically labeled cells. *Eur Biophys J*. 2002;31(2):118–125.
75. Allkemper T, Bremer C, Matuszewski L, Ebert W, Reimer P. Contrast-enhanced blood-pool MR angiography with optimized iron oxides: effect of size and dose on vascular contrast enhancement in rabbits. *Radiology*. 2002;223(2): 432–438.
76. Li W, Tutton S, Vu AT, et al. First-pass contrast-enhanced magnetic resonance angiography in humans using ferumoxytol, a novel ultrasmall superparamagnetic iron oxide (USPIO)-based blood pool agent. *J Magn Reson Imaging*. 2005;21(1): 46–52.
77. Berry I, Benderbous S, Ranjeva JP, Gracia-Meavilla D, Manelfe C, Le Bihan D. Contribution of Sinerem® used as blood-pool contrast agent: detection of cerebral blood volume changes during apnea in the rabbit. *Magn Reson Med*. 1996; 36(3):415–419.
78. Simonsen CZ, Østergaard L, Vestergaard-Poulsen P, Roehl L, Bjoernerud A, Gyldensted C. CBF and CBV measurements by USPIO bolus tracking: reproducibility and comparison with Gd-based values. *J Magn Reson Imaging*. 1999;9(2): 342–347.
79. Dunn JF, Roche MA, Springett R, et al. Monitoring angiogenesis in brain using steady-state quantification of ΔR2 with MION infusion. *Magn Reson Med*. 2004; 51(1):55–61.
80. Pouliquen D, Le Jeune JJ, Perdrisot R, Ermias A, Jallet P. Iron oxide nanoparticles for use as an MRI contrast agent: pharmacokinetics and metabolism. *Magn Reson Imaging*. 1991;9(3):275–283.
81. Weissleder R, Stark DD, Engelstad BL, et al. Superparamagnetic iron oxide: pharmacokinetics and toxicity. *Am J Roentgenol*. 1989;152(1):167–173.
82. Boni A, Ceratti D, Antonelli A, et al. USPIO-loaded red blood cells as a biomimetic MR contrast agent: a relaxometric study. *Contrast Media Mol Imaging*. 2014;9(3):229–236.
83. Antonelli A, Bruce IJ, Magnani M, Manuali E, Sfara C. Encapsulation of superparamagnetic nanoparticles into red blood cells as new carriers of MRI contrast agents. *Nanomedicine*. 2011;6:211–223.
84. Soler MA, Báo SN, Alcântara GB, et al. Interaction of erythrocytes with magnetic nanoparticles. *J Nanosci Nanotechnol*. 2007;7(3):1069–1071.
85. Antonelli A, Sfara C, Mosca L, Manuali E, Magnani M. New biomimetic constructs for improved in vivo circulation of superparamagnetic nanoparticles. *J Nanosci Nanotechnol*. 2008;8(5):2270–2278.
86. Markov DE, Boeve H, Gleich B, et al. Human erythrocytes as nanoparticle carriers for magnetic particle imaging. *Phys Med Biol*. 2010;55(21):6461.
87. Matsushita T, Kusakabe Y, Fujii H, Murase K, Yamazaki Y, Murase K. Inflammatory imaging with ultrasmall superparamagnetic iron oxide. *Magn Reson Imaging*. 2011;29(2):173–178.
88. Corot C, Petry KG, Trivedi R, et al. Macrophage imaging in central nervous system and in carotid atherosclerotic plaque using ultrasmall superparamagnetic iron oxide in magnetic resonance imaging. *Invest Radiol*. 2004;39(10):619–625.
89. Desestret V, Brisset JC, Moucharrafie S, et al. Early-stage investigations of ultrasmall superparamagnetic iron oxide-induced signal change after permanent middle cerebral artery occlusion in mice. *Stroke*. 2009;40(5):1834–1841.
90. Mori Y, Chen T, Fujisawa T, et al. From cartoon to real time MRI: in vivo monitoring of phagocyte migration in mouse brain. *Sci Rep*. 2014;4:6997.
91. Moore A, Marecos E, Bogdanov A Jr, Weissleder R. Tumoral distribution of long-circulating dextran-coated iron oxide nanoparticles in a rodent model 1. *Radiology*. 2000;214(2):568–574.
92. Tetsumura A, Nakamura S, Yoshino N, et al. USPIO-enhanced MRI of highly invasive and highly metastasizing transplanted human squamous cell carcinoma: an experimental study. *Dentomaxillofac Radiol*. 2012;41(1):55–63.
93. Kaluzova M, Bouras A, Machaidze R, Hadjipanayis CG. Targeted therapy of glioblastoma stem-like cells and tumor non-stem cells using cetuximab-conjugated iron-oxide nanoparticles. *Oncotarget*. 2015;6(11):8788–8806.
94. Yan F, Yang W, Li X, et al. Magnetic resonance imaging of atherosclerosis using CD81-targeted microparticles of iron oxide in mice. *Biomed Res Int*. 2015;2015: 758616.
95. von Elverfeldt D, von zur Muhlen C, Wiens K, et al. In vivo detection of activated platelets allows characterizing rupture of atherosclerotic plaques with molecular magnetic resonance imaging in mice. *PLoS One*. 2012;7(9):e45008.
96. Deddens LH, van Tilborg GA, van der Toorn A, et al. MRI of ICAM-1 upregulation after stroke: the importance of choosing the appropriate target-specific particulate contrast agent. *Mol Imaging Biol*. 2013;15(4):411–422.
97. Melemenidis S, Jefferson A, Ruparelia N, et al. Molecular magnetic resonance imaging of angiogenesis in vivo using polyvalent cyclic RGD-iron oxide microparticle conjugates. *Theranostics*. 2015;5(5):515–529.
98. Nighoghossian N, Wiart M, Berthezene Y. Novel applications of magnetic resonance imaging to image tissue inflammation after stroke. *J Neuroimaging*. 2008;18(4): 349–352.
99. Kleinschnitz C, Bendszus M, Frank M, Solymosi L, Toyka KV, Stoll G. In vivo monitoring of macrophage infiltration in experimental ischemic brain lesions by magnetic resonance imaging. *J Cereb Blood Flow Metab*. 2003;23(11): 1356–1361.
100. Saleh A, Wiedermann D, Schroeter M, Jonkmanns C, Jander S, Hoehn M. Central nervous system inflammatory response after cerebral infarction as detected by magnetic resonance imaging. *NMR Biomed*. 2004;17(4):163–169.
101. Walter HL, Walberer M, Rueger MA, et al. In vivo analysis of neuroinflammation in the late chronic phase after experimental stroke. *Neuroscience*. 2015; 292:71–80.
102. Deddens LH, Van Tilborg GAF, Mulder WJM, De Vries HE, Dijkhuizen RM. Imaging neuroinflammation after stroke: current status of cellular and molecular MRI strategies. *Cerebrovasc Dis*. 2012;33(4):392–402.
103. Bellinger DL, Lorton D, Felten SY, Felten DL. CHAPTER 14—macrophages in multiple sclerosis. *Immunobiology*. 1996;195(4–5):588–600.
104. Miller SD, Karpus WJ, Davidson TS. Experimental Autoimmune Encephalomyelitis in the Mouse. *Current Protocols in Immunology*: John Wiley & Sons, Inc.; 2001.
105. Nathoo N, Yong VW, Dunn JF. Understanding disease processes in multiple sclerosis through magnetic resonance imaging studies in animal models. *Neuroimage Clin*. 2014;4:743–756.
106. Millward JM, Schnorr J, Taupitz M, Wagner S, Wuerfel JT, Infante-Duarte C. Iron oxide magnetic nanoparticles highlight early involvement of the choroid plexus in central nervous system inflammation. *ASN Neuro*. 2013;5(1):e00110.
107. Chin CL, Pai M, Bousquet PF, et al. Distinct spatiotemporal pattern of CNS lesions revealed by USPIO-enhanced MRI in MOG-induced EAE rats implicates the involvement of spino-olivocerebellar pathways. *J Neuroimmunol*. 2009;211(1–2): 49–55.
108. Tysiak E, Asbach P, Aktas O, et al. Beyond blood brain barrier breakdown—in vivo detection of occult neuroinflammatory foci by magnetic nanoparticles in high field MRI. *J Neuroinflammation*. 2009;6:20.
109. Wuerfel J, Tysiak E, Prozorovski T, et al. Mouse model mimics multiple sclerosis in the clinico-radiological paradox. *Eur J Neurosci*. 2007;26(1):190–198.
110. Floris S, Blezer EL, Schreibelt G, et al. Blood-brain barrier permeability and monocyte infiltration in experimental allergic encephalomyelitis: a quantitative MRI study. *Brain*. 2004;127(pt 3):616–627.

111. Ladewig G, Jestaedt L, Misselwitz B, et al. Spatial diversity of blood–brain barrier alteration and macrophage invasion in experimental autoimmune encephalomyelitis: a comparative MRI study. *Exp Neurol*. 2009;220(1):207–211.
112. Rausch M, Hiestand P, Baumann D, Cannet C, Rudin M. MRI-based monitoring of inflammation and tissue damage in acute and chronic relapsing EAE. *Magn Reson Med*. 2003;50(2):309–314.
113. Crimi A, Commowick O, Maarouf A, et al. Predictive value of imaging markers at multiple sclerosis disease onset based on gadolinium- and USPIO-enhanced MRI and machine learning. *PLoS One*. 2014;9(4):e93024.
114. Dousset V, Brochet B, Deloire MS, et al. MR imaging of relapsing multiple sclerosis patients using ultra-small-particle iron oxide and compared with gadolinium. *AJNR Am J Neuroradiol*. 2006;27(5):1000–1005.
115. Tourdias T, Roggerone S, Filippi M, et al. Assessment of disease activity in multiple sclerosis phenotypes with combined gadolinium- and superparamagnetic iron oxide-enhanced MR imaging. *Radiology*. 2012;264(1):225–233.
116. Vellinga MM, Oude Engberink RD, Seewann A, et al. Pluriformity of inflammation in multiple sclerosis shown by ultra-small iron oxide particle enhancement. *Brain*. 2008;131(pt 3):800–807.
117. Nathoo N, Yong VW, Dunn JF. Using magnetic resonance imaging in animal models to guide drug development in multiple sclerosis. *Mult Scler*. 2014;20(1):3–11.
118. Deloire MS, Touil T, Brochet B, Dousset V, Caille JM, Petry KG. Macrophage brain infiltration in experimental autoimmune encephalomyelitis is not completely compromised by suppressed T-cell invasion: in vivo magnetic resonance imaging illustration in effective anti-VLA-4 antibody treatment. *Mult Scler*. 2004; 10(5):540–548.
119. Rausch M, Hiestand P, Foster CA, Baumann DR, Cannet C, Rudin M. Predictability of FTY720 efficacy in experimental autoimmune encephalomyelitis by in vivo macrophage tracking: clinical implications for ultrasmall superparamagnetic iron oxide-enhanced magnetic resonance imaging. *J Magn Reson Imaging*. 2004;20(1):16–24.
120. Foster-Gareau P, Heyn C, Alejski A, Rutt BK. Imaging single mammalian cells with a 1.5 T clinical MRI scanner. *Magn Reson Med*. 2003;49(5):968–971.
121. Townson JL, Ramadan SS, Simedrea C, et al. Three-dimensional imaging and quantification of both solitary cells and metastases in whole mouse liver by magnetic resonance imaging. *Cancer Res*. 2009;69(21):8326–8331.
122. Shi Q, Pisani LJ, Lee YK, et al. Evaluation of the novel USPIO GEH121333 for MR imaging of cancer immune responses. *Contrast Media Mol Imaging*. 2013; 8(3):281–288.
123. Roggendorf W, Strupp S, Paulus W. Distribution and characterization of microglia/macrophages in human brain tumors. *Acta Neuropathol*. 1996;92(3):288–293.
124. Fleige G, Nolte C, Synowitz M, Seeberger F, Kettenmann H, Zimmer C. Magnetic labeling of activated microglia in experimental gliomas. *Neoplasia*. 2001;3(6): 489–499.
125. Zimmer C, Wright SC Jr, Engelhardt RT, et al. Tumor cell endocytosis imaging facilitates delineation of the glioma–brain interface. *Exp Neurol*. 1997;143(1): 61–69.
126. Shevtsov MA, Nikolaev BP, Yakovleva LY, et al. Recombinant interleukin-1 receptor antagonist conjugated to superparamagnetic iron oxide nanoparticles for theranostic targeting of experimental glioblastoma. *Neoplasia*. 2015;17(1): 32–42.
127. Nasseri M, Gahramanov S, Netto JP, et al. Evaluation of pseudoprogression in patients with glioblastoma multiforme using dynamic magnetic resonance imaging with ferumoxytol calls RANO criteria into question. *Neuro Oncol*. 2014;16(8):1146–1154.
128. Gahramanov S, Muldoon LL, Varallyay CG, et al. Pseudoprogression of glioblastoma after chemo- and radiation therapy: diagnosis by using dynamic susceptibility-weighted contrast-enhanced perfusion MR imaging with ferumoxytol versus gadoteridol and correlation with survival. *Radiology*. 2013;266(3):842–852.
129. Varallyay CG, Muldoon LL, Gahramanov S, et al. Dynamic MRI using iron oxide nanoparticles to assess early vascular effects of antiangiogenic versus corticosteroid treatment in a glioma model. *J Cereb Blood Flow Metab*. 2009;29(4): 853–860.
130. Hussain SF, Yang D, Suki D, Aldape K, Grimm E, Heimberger AB. The role of human glioma-infiltrating microglia/macrophages in mediating antitumor immune responses. *Neurooncology*. 2006;8(3):261–279.
131. Yang I, Han SJ, Kaur G, Crane C, Parsa AT. The role of microglia in central nervous system immunity and glioma immunology. *J Clin Neurosci*. 2010;17(1): 6–10.
132. Sarkar S, Döring A, Zemp FJ, et al. Therapeutic activation of macrophages and microglia to suppress brain tumor-initiating cells. *Nat Neurosci*. 2014;17(1): 46–55.
133. Dekaban GA, Hamilton AM, Fink CA, et al. Tracking and evaluation of dendritic cell migration by cellular magnetic resonance imaging. *Wiley Interdiscip Rev Nanomed Nanobiotechnol*. 2013;5(5):469–483.
134. Baumjohann D, Hess A, Budinsky L, Brune K, Schuler G, Lutz MB. In vivo magnetic resonance imaging of dendritic cell migration into the draining lymph nodes of mice. *Eur J Immunol*. 2006;36(9):2544–2555.
135. Dósa E, Tuladhar S, Muldoon LL, Hamilton BE, Rooney WD, Neuwelt EA. MRI using ferumoxytol improves the visualization of central nervous system vascular malformations. *Stroke*. 2011;42(6):1581–1588.
136. Hasan DM, Amans M, Tihan T, et al. Ferumoxytol-enhanced MRI to image inflammation within human brain arteriovenous malformations: a pilot investigation. *Transl Stroke Res*. 2012;3(1):166–173.
137. Richards JM, Semple SI, MacGillivray TJ, et al. Abdominal aortic aneurysm growth predicted by uptake of ultrasmall superparamagnetic particles of iron oxide a pilot study. *Circ Cardiovasc Imaging*. 2011;4(3):274–281.
138. Hasan DM, Mahaney KB, Magnotta VA, et al. Macrophage imaging within human cerebral aneurysms wall using ferumoxytol-enhanced MRI: a pilot study. *Arterioscler Thromb Vasc Biol*. 2012;32(4):1032–1038.
139. Hasan D, Chalouhi N, Jabbour P, et al. Early change in ferumoxytol-enhanced magnetic resonance imaging signal suggests unstable human cerebral aneurysm a pilot study. *Stroke*. 2012;43(12):3258–3265.
140. Levitt MR, Kalani M, Moon K, McDougall CG, Albuquerque FC. Advances in the imaging of cerebral aneurysm inflammation. *Neuroimmunol Neuroinflammation*. 2015;2(2):51.
141. Friedrich RP, Janko C, Poettler M, et al. Flow cytometry for intracellular SPION quantification: specificity and sensitivity in comparison with spectroscopic methods. *Int J Nanomedicine*. 2015;10:4185–4201.
142. Shah RR, Davis TP, Glover AL, Nikles DE, Brazel CS. Impact of magnetic field parameters and iron oxide nanoparticle properties on heat generation for use in magnetic hyperthermia. *J Magn Magn Mater*. 2015;387:96–106.
143. Khot VM, Salunkhe AB, Ruso JM, Pawar SH. Improved magnetic induction heating of nanoferrites for hyperthermia applications: correlation with colloidal stability and magneto-structural properties. *J Magn Magn Mater*. 2015;384: 335–343.
144. Girard O, Ramirez R, McCarty S, Mattrey R. Toward absolute quantification of iron oxide nanoparticles as well as cell internalized fraction using multiparametric MRI. *Contrast Media Mol Imaging*. 2012;7(4):411–417.
145. Simon GH, Bauer J, Saborovski O, et al. T1 and T2 relaxivity of intracellular and extracellular USPIO at 1.5T and 3T clinical MR scanning. *Eur Radiol*. 2006;16(3):738–745.
146. Taylor A, Herrmann A, Moss D, et al. Assessing the efficacy of nano- and micro-sized magnetic particles as contrast agents for MRI cell tracking. *PLoS One*. 2014;9(6):e100259.
147. Danhier P, De Preter G, Boutry S, et al. Electron paramagnetic resonance as a sensitive tool to assess the iron oxide content in cells for MRI cell labeling studies. *Contrast Media Mol Imaging*. 2012;7(3):302–307.
148. Danhier P, De Preter G, Magat J, et al. Multimodal cell tracking of a spontaneous metastasis model: comparison between MRI, electron paramagnetic resonance and bioluminescence. *Contrast Media Mol Imaging*. 2014;9(2):143–153.
149. Fujiwara S, Uhrig L, Amadon A, Jarraya B, Le Bihan D. Quantification of iron in the non-human primate brain with diffusion-weighted magnetic resonance imaging. *Neuroimage*. 2014;102(pt 2):789–797.
150. Hardy PA, Gash D, Yokel R, Andersen A, Ai Y, Zhang Z. Correlation of R2 with total iron concentration in the brains of rhesus monkeys. *J Magn Reson Imaging*. 2005;21(2):118–127.
151. Wu EX, Tang H, Jensen JH. Applications of ultrasmall superparamagnetic iron oxide contrast agents in the MR study of animal models. *NMR Biomed*. 2004;17(7): 478–483.
152. Dennie J, Mandeville JB, Boxerman JL, Packard SD, Rosen BR, Weisskoff RM. NMR imaging of changes in vascular morphology due to tumor angiogenesis. *Magn Reson Med*. 1998;40(6):793–799.
153. Farrar CT, Kamoun WS, Ley CD, et al. In vivo validation of MRI vessel caliber index measurement methods with intravital optical microscopy in a U87 mouse brain tumor model. *Neurooncology*. 2010;11:2010.
154. Kim YR, Tejima E, Huang S, et al. In vivo quantification of transvascular water exchange during the acute phase of permanent stroke. *Magn Reson Med*. 2008; 60(4):813–821.
155. Seppenwoolde JH, Viergever MA, Bakker CJ. Passive tracking exploiting local signal conservation: the white marker phenomenon. *Magn Reson Med*. 2003;50(4): 784–790.
156. Kwon HJ, Shim WH, Cho G, et al. Simultaneous evaluation of vascular morphology, blood volume and transvascular permeability using SPION-based, dual-contrast MRI: imaging optimization and feasibility test. *NMR Biomed*. 2015;28(6):624–632.
157. Girard OM, Du J, Agemy L, et al. Optimization of iron oxide nanoparticle detection using ultrashort echo time pulse sequences: comparison of T1, T2*, and synergistic T1- T2* contrast mechanisms. *Magn Reson Med*. 2011;65(6):1649–1660.
158. Han SH, Cho JH, Jung HS, et al. Robust MR assessment of cerebral blood volume and mean vessel size using SPION-enhanced ultrashort echo acquisition. *Neuroimage*. 2015;112:382–389.
159. Engberink RDO, van der Pol SM, Döpp EA, de Vries HE, Blezer EL. Comparison of SPIO and USPIO for in vitro labeling of human monocytes: MR detection and cell function. *Radiology*. 2007;243(2):467–474.

160. Smith CE, Ernenwein D, Shkumatov A, et al. Hydrophilic packaging of iron oxide nanoclusters for highly sensitive imaging. *Biomaterials*. 2015;69: 184–190.
161. Shapiro EM, Skrtic S, Koretsky AP. Sizing it up: cellular MRI using micron-sized iron oxide particles. *Magn Reson Med*. 2005;53(2):329–338.
162. Wu YL, Ye Q, Foley LM, et al. In situ labeling of immune cells with iron oxide particles: an approach to detect organ rejection by cellular MRI. *Proc Natl Acad Sci U S A*. 2006;103(6):1852–1857.
163. Kim SJ, Lewis B, Steiner M-S, Bissa UV, Dose C, Frank JA. Superparamagnetic iron oxide nanoparticles for direct labeling of stem cells and in vivo MRI tracking [Published ahead of print (Aug 2015)]. *Contrast Media & Molecular Imaging*. 2015. doi: 10.1002/cmmi.1658
164. Bourrinet P, Bengele HH, Bonnemain B, et al. Preclinical safety and pharmacokinetic profile of ferumoxtran-10, an ultrasmall superparamagnetic iron oxide magnetic resonance contrast agent. *Invest Radiol*. 2006;41(3):313–324.
165. Wang Y-XJ. Superparamagnetic iron oxide based MRI contrast agents: current status of clinical application. *Quant Imaging Med Surg*. 2011;1(1):35–40.
166. Administration UFaD. *Feraheme (Ferumoxytol): Drug Safety Communication—Warnings Strengthened and Prescribing Instructions Changed*. 2015. Available at: http://www.fda.gov/Safety/MedWatch/SafetyInformation/SafetyAlertsforHumanMedicalProducts/ucm440479.htm
167. Liu W, Frank JA. Detection and quantification of magnetically labeled cells by cellular MRI. *Eur J Radiol*. 2009;70(2):258–264.
168. Srinivas M, Heerschap A, Ahrens ET, Figdor CG, de Vries IJM. (19)F MRI for quantitative in vivo cell tracking. *Trends Biotechnol*. 2010;28(7):363–370.
169. Flögel U, Ding Z, Hardung H, et al. In vivo monitoring of inflammation after cardiac and cerebral ischemia by fluorine magnetic resonance imaging. *Circulation*. 2008;118(2):140–148.
170. Kaneda MM, Caruthers S, Lanza GM, Wickline SA. Perfluorocarbon nanoemulsions for quantitative molecular imaging and targeted therapeutics. *Ann Biomed Eng*. 2009;37(10):1922–1933.
171. Ardenkjaer-Larsen JH, Fridlund B, Gram A, et al. Increase in signal-to-noise ratio of >10,000 times in liquid-state NMR. *Proc Natl Acad Sci U S A*. 2003;100(18):10158–10163.
172. Klippel S, Döpfert J, Jayapaul J. Cell tracking with caged xenon: using cryptophanes as MRI reporters upon cellular internalization. *Angew Chem Int Ed*. 2014;53(2): 493–496.
173. Wilson DM, Kurhanewicz J. Hyperpolarized 13C MR for molecular imaging of prostate cancer. *J Nucl Med*. 2014;55(10):1567–1572.
174. Rohrer M, Bauer H, Mintorovitch J, Requardt M, Weinmann H-J. Comparison of magnetic properties of MRI contrast media solutions at different magnetic field strengths. *Invest Radiol*. 2005;40(11):715–724.
175. Hamilton BE, Nesbit GM, Dosa E, et al. Comparative analysis of ferumoxytol and gadoteridol enhancement using T1- and T2-weighted MRI in neuroimaging. *AJR Am J Roentgenol*. 2011;197(4):981–988.
176. Szpak A, Fiejdasz S, Prendota W, et al. T1–T2 dual-modal MRI contrast agents based on superparamagnetic iron oxide nanoparticles with surface attached gadolinium complexes. *J Nanoparticle Res*. 2014;16(11):1–11.
177. Schmitt P, Griswold MA, Jakob PM, et al. Inversion recovery TrueFISP: quantification of T(1), T(2), and spin density. *Magn Reson Med*. 2004;51(4):661–667.
178. Chavhan GB, Babyn PS, Thomas B, Shroff MM, Haacke EM. Principles, techniques, and applications of T2*-based MR imaging and its special applications. *Radiographics*. 2009;29(5):1433–1449.